THE ASTROPHYSICAL JOURNAL, 392:602–615, 1992 June 20

HIGH-VELOCITY HCO^+ EMISSION ASSOCIATED WITH THE DR 21 MOLECULAR OUTFLOW

ROGNVALD P. GARDEN[1]
Department of Physics, University of California, Irvine, CA 92717
AND
JOHN E. CARLSTROM
Division of Physics, Mathematics, and Astronomy, MS 105-24, California Institute of Technology, Pasadena, CA 91125
Received 1991 September 12; accepted 1991 December 26

ABSTRACT

We have used the Hat Creek millimeter interferometer to study the spatial and velocity distribution of HCO^+ $J = 1$–0 line emission from the DR 21 young stellar outflow. The HCO^+ emission appears to arise from two spatially distinct components: (1) low-velocity clumps bordering the central DR 21 compact H II region, and (2) extended high-velocity gas associated with the DR 21 outflow lobes. The low-velocity emission probably arises from preexisting clumps of ambient gas that have been swept up and compressed by the slowly expanding compact H II region. The high-velocity HCO^+ emission associated with the outflow lobes exhibits a remarkable spatial correlation with the distribution of shock-excited H_2 line emission and is most likely formed by the compression and acceleration of ambient gas on interaction with a powerful young stellar wind. We argue that the observed spatial correlation between the HCO^+ and H_2 line emission results from two interrelated effects: (1) a small enhancement in the fractional abundance of HCO^+ in the shocked gas, and (2) the more favorable conditions for excitation of the HCO^+ ion in the warm, dense gas that comprises the outflow lobes. The velocity field internal to the western outflow lobe suggests that collisions between the outflow and dense clumps in the ambient cloud medium play an important role in orchestrating the dynamical evolution of this particular outflow lobe. We estimate remarkably large values for both the mass ($1100 \rightarrow 2670\ M_\odot$) and kinetic energy ($1 \rightarrow 2 \times 10^{48}$ ergs) of the DR 21 outflow, in good agreement with earlier estimates derived from measurements of CO line emission. Our observations therefore suggest that the DR 21 outflow source is one of the largest, most massive and energetic young stellar outflows discovered to date.

Subject headings: ISM: individual (DR 21) — ISM: jets and outflows — ISM: molecules

1. INTRODUCTION

The DR 21 compact H II region/molecular cloud core is one of the more luminous star-forming regions in the Galaxy ($\sim 6 \times 10^5\ L_\odot$: Harvey, Campbell, & Hoffman 1977; Campbell et al. 1982). At a distance of 3 kpc (Campbell et al. 1982), the DR 21 compact H II region is an intense radio continuum source consisting of at least six compact, high-density ionized components (A–F), whose free-free emission is equivalent to that of two O6, two O8, and two O9 main-sequence stars (Dickel et al. 1986; Roelfsema, Goss, & Geballe 1989). The compact O-star cluster appears to be confined within a more diffuse ionized component which extends $\sim 70''$ to the east of the compact H II region, and exhibits a sharp cut-off to the west (Harris 1973). Interferometric observations of H_2CO (Dickel et al. 1983; Dickel et al. 1986) and HCN (Dickel, Ho, & Wright 1985), in combination with the detection of a slight redshift in radio recombination line emission (Roelfsema et al. 1989), suggest that the H II region is a "blister" on the far side of the DR 21 molecular cloud. Additional evidence in support of this claim derives from the large value of the foreground extinction to the compact H II region ($A_v > 100$ mag) as determined from the measurement of infrared recombination-line decrements (Righini-Cohen, Simon, & Young 1979). It is therefore hardly surprising that the luminous O-stars which excite the DR 21 H II region are completely obscured at visible and infrared wavelengths (Harvey et al. 1986; Garden, Russell, & Burton 1990).

The first indication of outflow activity within the DR 21 molecular cloud complex derived from the discovery of broad wings (FWZI ~ 60 km s^{-1}) in low-J rotational CO spectra (Dickel, Dickel, & Wilson 1978; Phillips et al. 1981; Richardson et al. 1985). Furthermore, the presence of two emission components in the CO spectra indicated the existence of more than one molecular cloud along the same line of sight. The brightest emission component peaks at $v_{lsr} = -2.5$ km s^{-1} and is associated with the DR 21/W75S molecular cloud complex; the broad wings appear to be connected with this component. The second emission component, which lies at $v_{lsr} = 9$–11 km s^{-1}, is considerably weaker than the DR 21/W75S component and is most likely associated with the outer envelope of the W75N molecular cloud which lies $\sim 30'$ north of the DR 21 cloud core. Subsequent low angular resolution observations in the $J = 1$–0 line of CO (Fischer et al. 1985) partially resolved the DR 21 outflow into red- and blueshifted, high-velocity outflow lobes centered on the DR 21 H II region, although the redshifted lobe was difficult to define due to contamination by emission from the foreground W75N component.

More recently, the DR 21 molecular outflow has been studied at higher angular resolution in the infrared using the $v = 1$–0 $S(1)$ line of shock-excited molecular hydrogen (H_2) (Garden et al. 1986, 1990, 1991a) and at millimeter wavelengths in the $J = 1$–0 line of CO (Garden et al. 1991b). Together, these observations suggest that the DR 21 molecular outflow is poss-

[1] Alfred P. Sloan Fellow.

ibly the largest (extends over a projected distance of ~ 5 pc on the sky), most massive ($\sim 3000\ M_\odot$) and energetic ($\sim 2 \times 10^{48}$ ergs) young stellar outflow yet discovered in the Galaxy. Images of shock-excited H_2 $v = 1$–0 $S(1)$ line emission, obtained using an infrared camera with an angular resolution of $\sim 1''$ (Garden et al. 1990), clearly show that the DR 21 outflow lobes are composed of two highly-collimated jets of shocked molecular gas that are extremely clumpy and appear to become more focused with increasing distance from the outflow origin. Additional higher spectral resolution measurements of the H_2 $S(1)$ line at selected peaks of H_2 emission in both jets indicate that the shocked gas is moving at radial velocities in excess of 100 km s^{-1}. After deprojection, this gives actual velocities along the jet of order 200 km s^{-1} (Garden et al. 1991a).

Although infrared observations of shock-excited H_2 line emission provide high angular resolution, limitations in current technology preclude high spectral resolution; $\Delta v \approx 10$ km s^{-1} at the very best. Spectroscopy in the infrared thus gives a rather poor representation of the dynamics of the outflow gas. However, at millimeter wavelengths, the converse applies; it is easy to achieve high spectral resolution but difficult to match the high angular resolution of infrared cameras. The trade-off between high spectral and spatial resolution has relaxed somewhat over the past few years following the introduction of millimeter interferometers. With a millimeter interferometer it is now possible to make high spectral resolution measurements at angular resolutions close to those achievable at infrared wavelengths. In light of this fact, and driven by the desire to obtain a more detailed picture of the velocity structure of the DR 21 outflow lobes, we have undertaken a study of the DR 21 region in the $J = 1$–0 transition of HCO^+ using the Hat Creek millimeter interferometer array.

There are several reasons for choosing HCO^+ as the millimeter probe. First, it has been suggested that the fractional abundance of HCO^+ may be enhanced in the partially ionized gas following a strong shock (Dickinson et al. 1980; Elitzur 1983; White et al. 1987); we may therefore expect a close spatial correlation between the shock-excited H_2 and HCO^+ line emission. Second, the high critical density required for excitation of the $J = 1$–0 transition of HCO^+ ($n_{crit} \approx 10^5$ cm^{-3}) makes this line an ideal probe of dense molecular clumps both within and around the high-velocity outflow. By measuring the motions of these clumps, it should be possible to study the mechanics of the interaction between the outflow and the surrounding ambient cloud. Finally, the detection of extended, high-velocity HCO^+ emission toward other luminous outflow sources, such as Orion KL (Vogel et al. 1984), NGC 2071 (Wootten et al. 1984; Kitamura et al. 1990), Ceph A (Loren et al. 1984), and NGC 7538 IRS 1 (Pratap, Batrla, & Snyder 1990) provides empirical proof that the HCO^+ emission is both bright and ubiquitous, being an ideal probe of dense gas within both the dense star-forming cores and the extended high-velocity outflow lobes.

The observations are discussed in § 2. The results are presented in § 3 and discussed in § 4. Finally, we summarize our main conclusions in § 5.

2. OBSERVATIONS

The HCO^+ $J = 1$–0 (89.18852 GHz) observations of the DR 21 outflow source were made between 1988 May and 1988 November using the Hat Creek millimeter interferometer array[2]. A total of 11 configurations of the three 6.1 m antennas were used, resulting in 22 nonredundant baselines providing u-v coverage spanning from 1.8 to 29 kλ. Because of the large extent of the DR 21 outflow ($\sim 5'$ on the sky: Garden et al. 1986), three fields were observed, centered on (1) the DR 21 cloud core/outflow center ($0^s.0$, $0'' = 20^h37^m14^s.0$, $+42°08'58''$), (2) the eastern outflow lobe ($+5^s.9$, $+24''$), and (3) the western outflow lobe ($-5^s.9$, $-24''$). The $70''$ offset between field centers corresponds to half of the $2'.3$ primary beam and therefore provided good sensitivity in the region of overlap. Strong HCO^+ emission was found in all three fields, centered at the DR 21 cloud rest velocity, $v_{lsr} \approx -2.5$ km s^{-1}. The observation cycle consisted of 10 minute observations toward each field and then the phase calibrator 2037+511. Additional observations of 3C 273, 3C 84, and 3C 454 were used to measure the passband gains and also to check the antenna gains and baseline solutions. Observations of Mars and Venus were used to establish the absolute flux density scale, which should be accurate to approximately 25%. The single sideband system temperatures scaled to above the atmosphere were typically 270–500 K.

The data were processed using the RALINT software package developed by the Radio Astronomy Laboratory at the University of California, Berkeley. Maps of HCO^+ emission from the individual fields were made and CLEANed separately. The u-v data were weighted to achieve high sensitivity to low surface brightness emission, resulting in nearly identical (within $0''.1$) $10''.4 \times 9''.4$ at p.a. $\sim 90°$ beams for all three fields. Integrated intensity maps of the separate fields were made by combining the channels maps with a 1.5 σ (0.2 Jy beam^{-1}) threshold. These maps were corrected for the primary beam response and then mosaicked[3] where the weight of each pixel was set by the primary beam response (pixels for which the primary beam response was less than 0.5 were not used). The noise level is therefore not uniform across the mosaicked maps; it is higher at the edge of the map due to the primary beam correction and lower in the regions of overlap due to the increased integration time.

The spectrometer was configured to obtain continuum data in a 40 MHz bandwidth passband, free from line emission in the same sideband as the HCO^+ emission. Maps of these data were made with the same u-v weighting as for HCO^+ data for subtraction from the line+continuum maps. In addition, we made a higher resolution map of the continuum emission with a $5''.6 \times 5''.3$ at p.a. 88° beam. Continuum emission was detected only from the luminous DR 21 compact H II region.

3. RESULTS

3.1. 89 *Gigahertz Continuum*

At the heart of the DR 21 molecular cloud lies the DR 21 compact H II region which is an extremely bright radio continuum source. In Figure 1 we present a map of the 89 GHz ($\lambda = 3.36$ mm) continuum emission, as discussed in § 2. The morphology of the 89 GHz continuum is almost identical to that exhibited at 15 GHz (Roelfsema et al. 1989; Dickel et al. 1986). The southern peak with the slight northern extension is

[2] The Hat Creek millimeter interferometer is operated by the Berkeley-Illinois-Maryland Association (BIMA), with support from the National Science Foundation.

[3] Here we use the term mosaicking to refer to the technique described above in which the images of the three fields are combined after CLEANing. We did not use a mosaicking method in which the u-v data are combined.

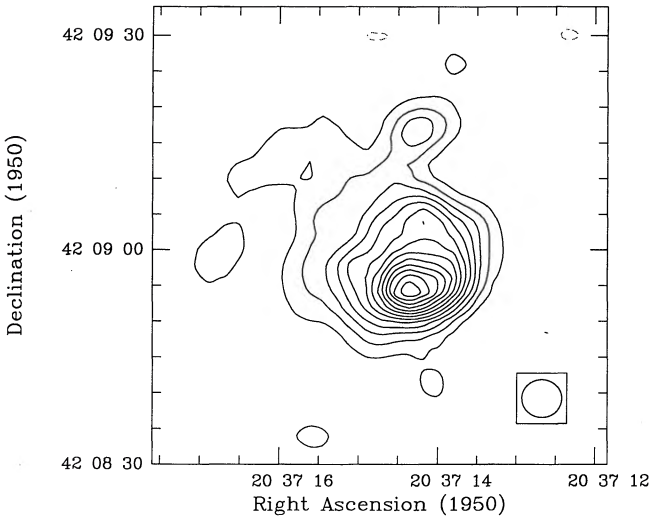

FIG. 1.—Contours of 89 GHz ($\lambda = 3.36$ mm) continuum emission toward the DR 21 compact H II region. The contours are multiples of 0.150 Jy beam^{-1} starting at ± 0.150 Jy beam^{-1} and the FWHM contour of the synthesized beam shown in the bottom right corner is 5".6 × 5".3 at p.a. 88°.

known to be composed of three spatially distinct components: A, B, and C (Harris 1973; Roelfsema et al. 1989). Unfortunately, these components are poorly resolved at the angular resolution ($\sim 6''$) of the current observations. The northern peak in Figure 1 is associated with component D. Components B and C each have an ionizing flux equivalent to that of an O6 ZAMS star while the ionizing fluxes of components A and D are equivalent to those of ZAMS stars of type O8. The two remaining components, E and F, form a weak eastward extension to the DR 21 compact H II region that is difficult to see in our 89 GHz continuum map but is clearly evident in the higher signal-to-noise ratio 15 GHz map presented by Roelfsema et al. In total, the ionizing flux associated with the DR 21 H II region is equivalent to that of ~ 11 O8 ZAMS stars. There is no doubt, therefore, that we are witnessing the formation of a young O-star cluster in this region.

We measure an integrated continuum flux of ~ 18.6 Jy at 89 GHz compared to 17.5 and 18.3 Jy at 5 and 15 GHz, respectively (Roelfsema et al.). The almost flat spectral index strongly suggests that most of the continuum emission measured at 89 GHz is pure free-free radiation associated with the DR 21 H II region. We note that, although the emission at significantly shorter wavelengths [$S(1100\ \mu m) = 110$ Jy and $S(800\ \mu m) = 435$ Jy] appears to be consistent with optically thin emission from cold dust grains (Richardson, Sandell, & Krisciunas 1989), this cold dust emission should contribute only ~ 1 Jy at 89 GHz ($\lambda = 3.36$ mm). It is also worth noting that the submillimeter continuum is elongated in a N-S direction which is approximately orthogonal to the E-W axis of the DR 21 high-velocity outflow (see below). It is thus most likely that the submillimeter continuum traces a dense ridge of cool gas which perhaps acts as a crude collimating agent for the DR 21 outflow.

3.2. HCO^+ *Velocity-Channel Maps*

Velocity-channel maps of the continuum-subtracted HCO^+ mosaic of the east, center, and west fields are displayed in Figure 2. In making these maps, the line emission was integrated over 5 km s^{-1} intervals, thus improving the sensitivity to extended, high-velocity emission. The excess negative contours in the low-velocity channel maps compared to the high-velocity maps indicate that the interferometer resolved out an extended low-velocity component, detecting only the brighter clumps of the low-velocity emission.

The velocity-channel maps show several interesting features:

1. Extended, high-velocity HCO^+ emission is clearly detected from both the east and west fields, extending to more than ± 30 km s^{-1} from the DR 21 rest velocity ($v_{lsr} \approx -2.5$ km s^{-1}). As we shall discuss below, the high-velocity emission from the east and west fields is probably associated with the outflow lobes of a high-velocity stellar wind that originates from within the DR 21 cloud core.

2. The brightest emission at low velocities (-10 to 0 km s^{-1}) comes from the central field, taking the form of several bright clumps arranged in a partial ring with the brightest clump lying a few arcseconds to the southwest of the field center. This southwestern clump is probably the same high-density clump previously detected by Dickel et al. (1986) in HCN $J = 1$–0 emission and Keto (1990) in NH_3 line emission. As will be discussed further in § 4.1, a logical explanation for the ringlike appearance of the central source is that it may result from the sweeping-up of the ambient cloud material by the slowly expanding DR 21 H II region.

3. The high-velocity HCO^+ emission from the east and west fields originates from several distinct clumps which become more numerous as the velocity offset approaches the cloud rest velocity. Contrary to what is found in the east and west fields, there is an apparent lack of high-velocity emission from the central field. In addition, the central source appears to be separated from the high-velocity outflow lobes by regions of significantly weaker HCO^+ line emission. It is interesting to note that a similar gap toward the innermost parts of the DR 21 outflow lobes is also seen in shock-excited H_2 line emission (Garden et al. 1991a).

4. A bright negative peak of emission is seen toward the central field at $v_{lsr} \approx 10$ km s^{-1}. This negative peak results from the absorption of continuum photons from the DR 21 compact H II region by the outer envelope of the W75N molecular cloud which lies in front of the DR 21 cloud and is known to have a rest velocity of $v_{lsr} = 9$–11 km s^{-1} (Dickel et al. 1978).

In order to obtain a clearer picture of the morphology of the HCO^+ emission, we have summed the individual velocity-channel maps (-40 to 25 km s^{-1}), resulting in the map of integrated HCO^+ line emission displayed in Figure 3. The most striking feature in this map is the bipolar configuration of the east and west lobes and their symmetry with respect to the central ringlike source. The HCO^+ emission extends for more than 4' in the plane of the sky which, at a distance of 3 kpc, corresponds to a source length of ~ 4 pc. A similar bipolar morphology has previously been detected in H_2 (Garden et al. 1986; Garden et al. 1991a), CO (Garden et al. 1991b), CS and HCN (Garden 1987) line emission. We aim to show in this paper that the similar bipolar morphology exhibited by these five different molecular species constitutes convincing evidence in favor of a model in which the twin-lobed morphology results from an unusually energetic young stellar wind which, on interaction with the surrounding ambient cloud medium, creates two large and massive outflows of shock-heated, swept-up ambient gas.

Figure 4 shows examples of HCO^+ $J = 1$–0 spectra at several positions in the outflow lobes and the central source as indicated in Figure 3. The spectra associated with the outflow

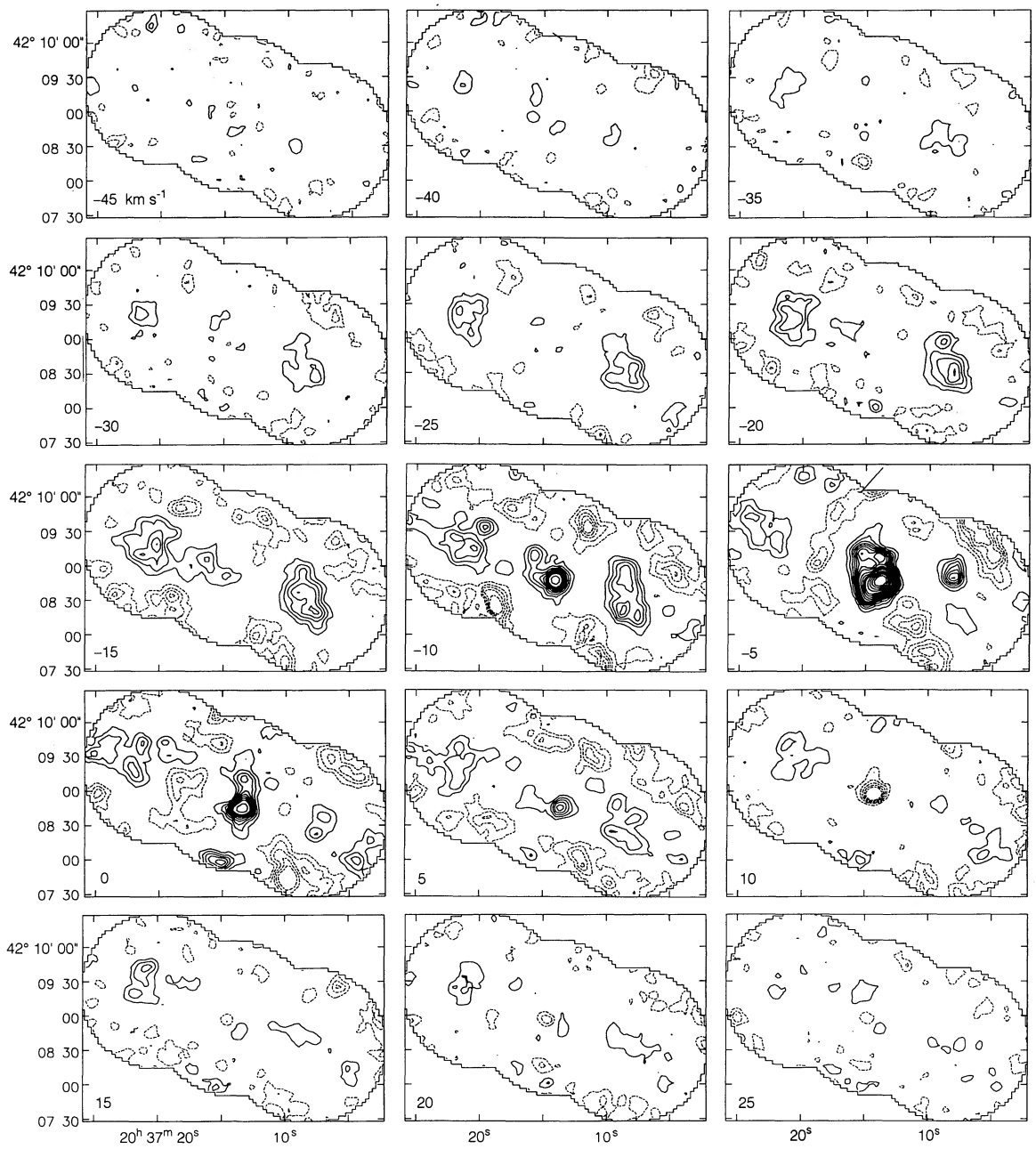

FIG. 2.—Continuum-subtracted velocity-channel mosaics of the HCO^+ $J = 1$–0 emission from the east, center, and west fields. The line emission is averaged over 5 km s^{-1} intervals. The center velocity is shown in the bottom left corner of each panel. The contours are 0.30 Jy $beam^{-1}$ × −5, −4, −3, −2, −1, 1, 2, 3, 4, 5, 6, 7, 8, 10, 12, 14, 16, 20, 24, 28, 32. The beam size is 10″.3 × 9″.4 at p.a. 96° and 1 Jy $beam^{-1}$ equals 1.59 K.

lobes (i.e., spectra 1, 2, 4, 5, and 6) have reasonably broad profiles with well-defined high-velocity wings while the spectrum of the central source (i.e., spectrum 3) is characterized by an extremely narrow, wingless profile. Another dynamical feature worthy of mention is the sudden change from primarily blueshifted emission halfway down the western lobe (spectrum 5) to predominantly redshifted emission at the end of this lobe (spectrum 6). This particularly interesting result agrees with previous velocity measurements of H_2 (Garden et al. 1991a) and CO (Garden et al. 1991b) line emission and may be attributed to the bending of the outflow following a collision with a dense clump in the ambient molecular cloud. The interaction between the DR 21 molecular outflow and the surrounding ambient cloud medium is discussed further in § 4.4. As a final observation we note that, in contrast to the vast majority of outflow sources observed to date, the DR 21 HCO^+ outflow lobes *do not appear to be bipolar in velocity*; i.e., there is no well-defined redshift or blueshift between the eastern and western outflow lobes. If anything, the bulk of the emission from both lobes appears to be primarily blueshifted by ∼15 km s^{-1} from the DR 21 cloud rest velocity. The lack of bipolarity is puzzling but may just reflect the fact that the outflow

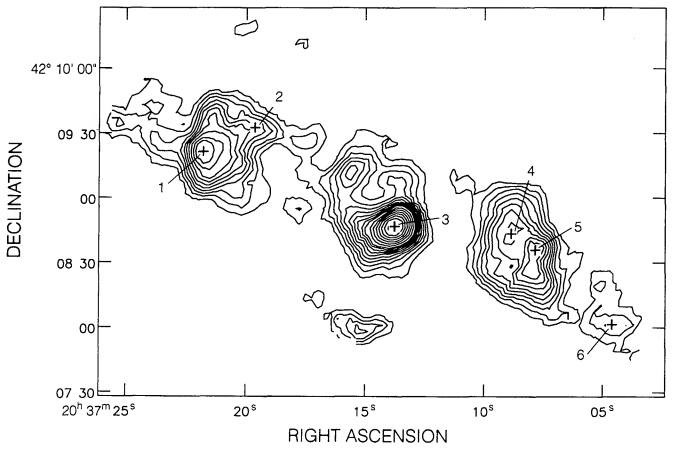

FIG. 3.—Mosaic of the total integrated intensity of HCO^+ $J = 1$–0 from the east, center, and west fields. The emission is integrated from −40 to +20 km s^{-1}. The beam size is 10.″3 × 9.″4. The contours are 3.6 Jy km s^{-1} $beam^{-1}$ × 1, 2, 3, 4, 5, 6, 7, 8, 9, 10, 12, 14, 16, 18, 20, 22, 24, and 1 Jy km s^{-1} $beam^{-1}$ equals 1.59 K km s^{-1}. Also shown are the positions corresponding to the numbered spectra in Fig. 4.

axis is aligned almost in the plane of the sky, resulting in small projected radial velocity shifts.

3.3. HCO^+ *Line Optical Depth*

In order to calculate the column density and mass of the gas in the DR 21 outflow lobes, we first need to estimate the optical depth of the HCO^+ $J = 1$–0 line. The optical depth τ of a particular transition of a linear, rigid rotor molecule can be expressed as follows (see appendix of Garden et al. 1991b):

$$\int \tau\, dv = \frac{4\pi^3 \mu^2 \nu N_{\rm tot}}{3kT_{ex}} \exp\left(-\frac{Jh\nu}{2kT_{\rm ex}}\right)\left[1 - \exp\left(-\frac{h\nu}{kT_{\rm ex}}\right)\right], \quad (1)$$

where $N_{\rm tot}$ is the total column density of the molecule in all levels, μ is the dipole moment, and J corresponds to the lower level of the rotational transition $J + 1 \rightarrow J$. Note that for a Gaussian line profile, $\int \tau\, dv = \tau\, \Delta v/0.94$ (Lang 1980), where Δv is the full width half-maximum (FWHM) of the profile. However, as the shape of the line profile is not precisely known, we shall simply approximate the integral by $\int \tau\, dv \approx \tau\, \Delta v$. For the $J = 1$–0 transition of HCO^+, the optical depth is therefore given by

$$\tau(HCO^+) = 5.33 \times 10^{-12} \frac{N(H_2)X(HCO^+)}{\Delta v T_{\rm ex}} \times \left[1 - \exp\left(-\frac{4.28}{T_{\rm ex}}\right)\right], \quad (2)$$

where we have used $\mu = 4.48$ D (Blake et al. 1987; taken from Haese & Woods 1979), Δv is expressed in km s^{-1}, and $X(HCO^+)$ is the fractional abundance of HCO^+ relative to H_2. When comparing our results with those of other authors it is important to note that most papers written earlier than 1987 used a significantly lower value for the dipole moment, usually $\mu = 3.3$ D.

An upper limit to the optical depth of the HCO^+ $J = 1$–0 line toward the DR 21 outflow lobes can be estimated from the peak molecular hydrogen column density, as inferred from the nondetection of $C^{18}O$ emission from the DR 21 outflow lobes: $N(H_2) < 5 \times 10^{22}$ cm^{-2} (Garden et al. 1991b). Garden et al. (1986) deduce a similar value for the molecular hydrogen column density toward the DR 21 outflow lobes [$N(H_2) \approx 3 \times 10^{22}$ cm^{-2}] using an estimate of the visual extinction as derived from the intensity ratio of two different lines of vibrationally excited molecular hydrogen (see also Nadeau, Riopel, & Geballe 1991). For the excitation temperature, we obtain a crude estimate by using the peak radiation temperature of the thermalized ^{12}CO line: $T_{\rm ex} \approx 30$ K (Garden et al. 1991b). Also, considering the large width of the HCO^+ lines associated with

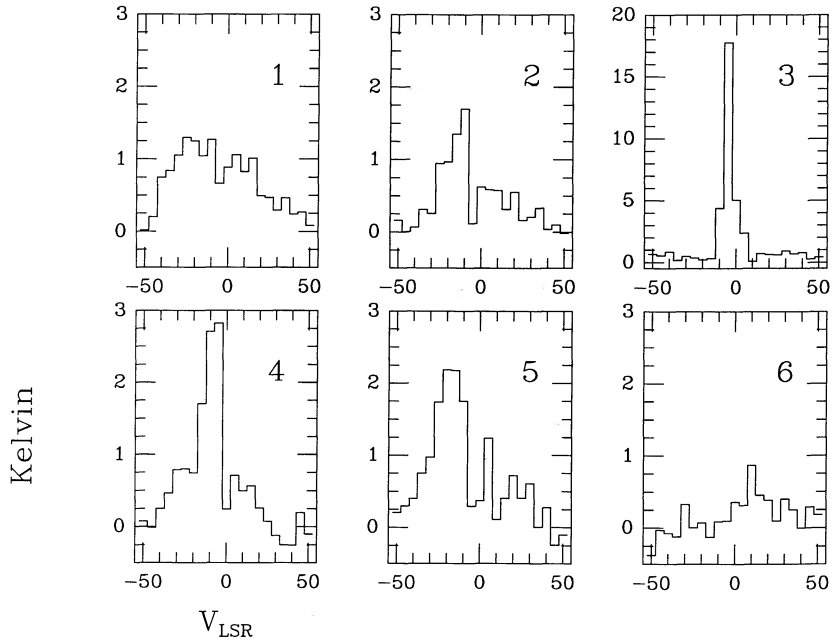

FIG. 4.—Selected HCO^+ $J = 1$–0 spectra at several positions in the outflow lobes and central source, as shown in Fig. 3. The intensity scale is expressed in K, and the velocity scale in km s^{-1}.

the outflow lobes, we use $\Delta v > 10$ km s^{-1} for the FWHM of the line. Finally, for the fractional abundance, we use $X(HCO^+) < 10^{-8}$, as estimated in § 3.5. For the above limits, equation (2) gives $\tau(HCO^+) < 1$ as a conservative upper limit for the optical depth of the HCO^+ $J = 1$–0 line toward the DR 21 outflow lobes. Thus, we shall assume from here on that the HCO^+ $J = 1$–0 line is optically thin at all velocities in both outflow lobes. We note, however, that this assumption does *not* apply for emission from the DR 21 cloud core (i.e., the central source) where measurements of the $H^{13}CO^+$ isotope (Garden, Russell, & Hayashi 1992) show the HCO^+ $J = 1$–0 line to be optically thick.

3.4. *Beam-averaged Column Density*

Using equation (1), the total column density N_{tot} of a rigid, rotor molecule of dipole moment μ can be calculated from observations of a rotational transition $J + 1 \rightarrow J$ as follows

$$N_{tot} = \frac{3k}{4\pi^3 \mu^2 \nu} \times \frac{T_{ex}}{[1 - \exp(-h\nu/kT_{ex})] \exp(-Jh\nu/2kT_{ex})} \int \tau \, dv \, . \quad (3)$$

The beam-averaged total column density, $\bar{N}_{tot}$, is obtained by multiplying the above equation by the beam-filling factor $\mathcal{F}$ (see Fischer et al. 1985; Garden et al. 1991b):

$$\mathcal{F} = \frac{T_R}{\{(h\nu/k)[\exp(h\nu/kT_{ex}) - 1]^{-1} - (h\nu/k) \times [\exp(h\nu/kT_{bg}) - 1]^{-1}\}[1 - \exp(-\tau)]} , \quad (4)$$

where T_R is the radiation temperature measured from the source and where $T_{bg} \approx 2.73$ K is the temperature of the cosmic background radiation. In the limit $T_{ex} \gg T_{bg}$ the cosmic background radiation can be neglected, and the beam-averaged total column density is then given by

$$\bar{N}_{tot} = 6.96 \times 10^{15} \frac{T_{ex}}{\mu^2 \nu^2 \exp[(-h\nu/kT_{ex})(1 + J/2)]} \times \int \frac{T_A^*}{\eta_B} \frac{\tau}{[1 - \exp(-\tau)]} \, dv \, , \quad (5)$$

where the velocity v is expressed in km s^{-1}, the dipole moment μ in D, and the frequency ν in GHz. Note also that the radiation temperature T_R is now expressed in terms of the observed antenna temperature T_A^* and the beam efficiency η_B. For the $J = 1$–0 transition of HCO^+, $J = 0$, $\mu = 4.48$ D (see § 3.3), $\nu = 89.18852$ GHz, and we obtain

$$\bar{N}_{tot}(HCO^+) = 4.36 \times 10^{10} \frac{T_{ex}}{\exp(-4.28/T_{ex})} \times \int \frac{T_A^*}{\eta_B} \frac{\tau}{[1 - \exp(-\tau)]} \, dv \, . \quad (6)$$

It is worth noting that in the optically thin limit ($\tau \rightarrow 0$), the optical depth disappears from the above equation as $\tau/[1 - \exp(-\tau)] \approx 1$. The above equation will be used to calculate the total column density of molecular gas in § 3.6. However, before doing so, we first need to obtain an estimate for the fractional abundance of HCO^+.

3.5. *Fractional Abundance of* HCO^+

Having determined that the HCO^+ emission from the DR 21 outflow lobes is probably optically thin, we now proceed to calculate the fractional abundance of HCO^+, $X(HCO^+)$, in the outflow lobes. A measurement of $X(HCO^+)$ is important not only for calculating the total column density and mass of gas but also because it may reveal important changes in the cloud chemistry following the passage of a strong shock. For example, Iglesias & Silk (1978) have shown that the presence of shocks in molecular clouds can lead to a substantial decrease in $X(HCO^+)$ as a result of greater recombination in the dense postshock gas. Alternatively, Elitzur (1983) has shown that a fast shock can heat the postshock gas to a sufficiently high temperature that ionization may become more important than recombination, leading to an increase in $X(HCO^+)$. There have been several reports of enhanced $X(HCO^+)$ in clouds harboring strong shocks (Dickinson et al. 1980; White et al. 1987; Vogel et al. 1984; Lizano et al. 1988). However, there exist just as many reports claiming no enhancement (Wootten et al. 1984; Loren et al. 1984; Ziurys, Snell, & Dickman 1989). The question of whether $X(HCO^+)$ changes following the passage of a strong shock therefore remains largely unresolved.

More recently, Wolfire & Königl (1992) have proposed that an enhanced $X(HCO^+)$ can be produced in quiescent material which is illuminated by X-ray, EUV, and UV radiation produced in a nearby strong (i.e., $v_{shock} > 100$ km s^{-1}) shock. Their time-dependent model not only produces abundances of ionized molecular species that are several orders of magnitude greater than predicted in steady state models, but also suggests that collisional excitation of HCO^+ by electrons is important, even at relatively low ($n = 10^4 \rightarrow 10^5$ cm^{-3}) densities. Although this model was developed to explain the occurrence of HCO^+ emission in Herbig-Haro objects, it is tempting to suggest that it may also apply to the case of the DR 21 outflow lobes where shock velocities in excess of 100 km s^{-1} are known to exist from infrared observations of H_2 line profiles (Garden et al. 1991a).

One method for determining $X(HCO^+)$ in the postshock gas is to compare the column density of HCO^+ with the column density of another molecule whose fractional abundance is expected to be unchanged following the passage of a shock (e.g., Kuiper, Zuckerman, & Rodriguez-Kuiper 1981). In carrying out this analysis, it is best if one chooses two molecular lines that are expected to be optically thin and to originate from the same volume of gas. Probably the easiest line to use for such a comparison is the $J = 1$–0 transition of ^{13}CO, since the fractional abundance of the CO molecule is predicted to be relatively unaffected by high-temperature chemistry (Iglesias & Silk 1978). However, the large difference in dipole moments between the HCO^+ and CO molecules implies that the CO line is excited at much lower densities than HCO^+ and thus that the lines probably are formed in different regions. Ziurys et al. (1989) argue that HCN is a better comparison molecule than ^{13}CO as it has a dipole moment closer to that of HCO^+ and hence is expected to be excited under similar conditions. However, Mitchell (1984) has shown that $X(HCN)$ is more prone to be enhanced at elevated temperatures than $X(^{13}CO)$ which in itself could lead to erroneous results. In view of the above discussion, we have chosen to conduct our analysis of $X(HCO^+)$ using both the ^{13}CO and HCN lines, the rationale being that the actual value of $X(HCO^+)$ should lie somewhere between the limiting values obtained from these two lines.

The Nobeyama 45 m telescope was used to obtain a series of simultaneous HCO^+, HCN, and ^{13}CO spectra along a north-south cut through the peak of integrated HCO^+ emission in the western outflow lobe. The results of these observations, which are to be discussed in greater detail in a future paper

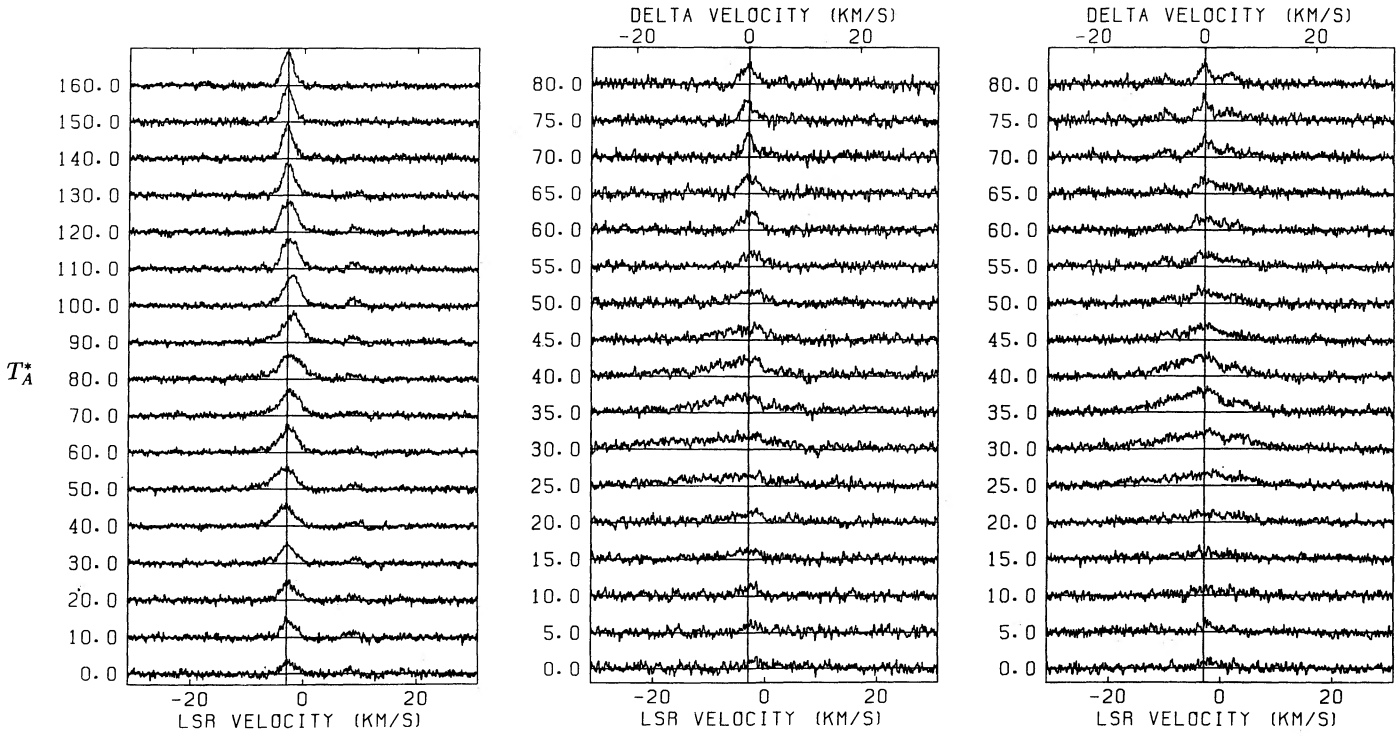

FIG. 5a FIG. 5b FIG. 5c

FIG. 5.—Spectra of ^{13}CO $J = 1–0$ (*a*), HCO^+ $J = 1–0$ (*b*), and HCN $J = 1–0$ (*c*) line emission along a N-S strip bisecting the western outflow lobe obtained using the Nobeyama 45 m telescope. The beam size was $\sim 16''$ at 110 GHz and $\sim 20''$ at 89 GHz. Adjacent spectra are separated by $15''$ on the sky.

(Garden et al. 1992), are shown in Figures 5*a*, 5*b*, and 5*c*. The beam size was measured to be $\sim 16''$ at 110 GHz and $\sim 20''$ at 89 GHz. In the quiescent cloud, at the top and bottom of each cut, all three lines are relatively narrow with line peaks centered on the systemic velocity of the DR 21 cloud (~ -2.5 km s^{-1}). However, toward the outflow lobe, close to the center of each cut, both the HCO^+ and HCN lines develop a bright blueshifted wing that is more than 10 times brighter than any corresponding ^{13}CO wing emission. One possible explanation for this striking difference is that the fractional abundance of both HCO^+ and HCN is significantly enhanced in the high-velocity, postshock gas relative to the ambient cloud medium. Alternatively, the enhanced high-velocity emission may result from a sudden change in excitation conditions between the ambient cloud and the outflow lobe that is felt more strongly by both the HCO^+ and HCN molecules than the ^{13}CO molecule, which is relatively insensitive to such changes due to its low dipole moment.

If we assume that for any pair of lines, both lines are (1) optically thin, (2) coextensive, and (3) have a common T_{ex}, a measure of the relative abundances can be obtained from a comparison of the respective integrated line temperatures (see eqs. [5] and [6]):

$$\frac{X(HCO^+)}{X(^{13}CO)} = \frac{\bar{N}_{tot}(HCO^+)}{\bar{N}_{tot}(^{13}CO)} = 8.9 \times 10^{-4} \times \frac{\int T_A^*(HCO^+ J = 1–0)dv}{\int T_A^*(^{13}CO J = 1–0)dv} \frac{\eta_B(110\ \text{GHz})}{\eta_B(89\ \text{GHz})}, \quad (7)$$

$$\frac{X(HCO^+)}{X(HCN)} = \frac{\bar{N}_{tot}(HCO^+)}{\bar{N}_{tot}(HCN)} = 0.44 \frac{\int T_A^*(HCO^+ J = 1–0)dv}{\int T_A^*(HCN J = 1–0)dv}, \quad (8)$$

where we have set $T_{ex} = 30$ K and have used $\mu = 4.48$, 2.98, and 0.11 D for the dipole moments of HCO^+, HCN, and ^{13}CO, respectively (Blake et al. 1987). Also, for the Nobeyama 45 m telescope, the beam efficiencies are taken to be $\eta_B(110\ \text{GHz}) = 0.36$ and $\eta_B(89\ \text{GHz}) = 0.44$, respectively. Note that the beam efficiencies are not needed in equation (8), since the HCN and HCO^+ line frequencies are less than 1 GHz apart.

Let us first calculate $X(HCO^+)$ assuming that the ^{13}CO and HCO^+ lines arise from the same volume of gas. The line emission is segmented into two distinct velocity components: a line-core component (-8 to 3 km s^{-1}) associated with the quiescent cloud, and a high-velocity wing component (-28 to -8 km s^{-1}) which traces the shocked outflow gas. The redshifted wing component was not used due to contamination by absorption/emission from the foreground W75N cloud. The relative abundance of HCO^+, as calculated using equation (7), is plotted in Figures 6*a* and 6*b* as a function of displacement along the north-south cut through the western outflow lobe. Clearly, the line-core component is relatively insensitive to the presence of the outflow lobe. However, the high-velocity wing component, for which only the positions where high-velocity ^{13}CO emission was detected are plotted, appears to peak on the outflow lobe, at which position $X(HCO^+)/X(^{13}CO)$ is about an order of magnitude larger than in the quiescent cloud, as reflected by the line-core component. Assuming a terrestrial abundance ratio of $X(^{13}CO) \approx 10^{-6}$, we find $4 \times 10^{-9} \leq X(HCO^+) \leq 8 \times 10^{-9}$ for the high-velocity wing component and $2 \times 10^{10} \leq X(HCO^+) \leq 5 \times 10^{-10}$ for the line-core component. This important result suggests that *if the* ^{13}CO *and* HCO^+ *lines originate from the same volume of gas,* then the fractional abundance of HCO^+ in the outflow is enhanced by at least a factor of 10, compared to the quiescent cloud. However, it is important to note that this would be an enhancement particular to the DR 21 cloud. Indeed, the peak

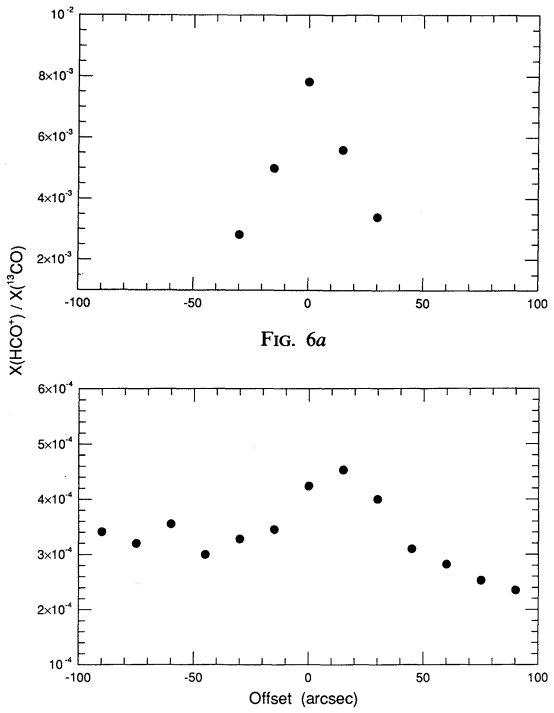

FIG. 6a

FIG. 6b

FIG. 6.—(*a*) Values of $X(HCO^+)/X(^{13}CO)$ for the high-velocity component (-28 to -8 km s^{-1}) measured along a N-S cut centered on the peak of high-velocity HCO^+ emission from the western outflow lobe. Only positions where high-velocity ^{13}CO emission was detected are plotted. (*b*) As for (*a*), but for the low-velocity component (-8 to 3 km s^{-1}).

$X(HCO^+)$ in the DR 21 outflow lobe is *not* unusual compared to other dark clouds, where $X(HCO^+)$ on the order of $10^{-9} \rightarrow 10^{-8}$ are commonplace (Ziurys et al. 1989). What is more unusual is the anomalously low value of $X(HCO^+)$ inferred for the DR 21 quiescent cloud.

Considering the accompanying enhancement in high-velocity HCN emission across the outflow lobe (see Fig. 5*c*), it is clear that the above estimate of $X(HCO^+)$, based on a comparison with the ^{13}CO line, is an overestimate as it does not take into account the fact that possible changes in excitation may be responsible for the increased HCO^+ line brightness. In this respect, a comparison with the relatively inert HCN molecule should prove useful. Because of the fine-structure splitting of the HCN line, it is difficult to conduct an analysis using different velocity components. Instead, the emission was integrated over the entire line profile (-28 to 20 km s^{-1}) and a velocity-averaged value for $X(HCO^+)/X(HCN)$ was calculated, as defined by equation (8), for each position along the north-south cut through the western outflow lobe. The result is plotted in Figure 7. In the quiescent cloud, at large displacements from the outflow lobe, we find $X(HCO^+)/X(HCN) \approx 0.2$. However, on passing through the outflow lobe this ratio steadily increases to a peak value of ~ 0.6. We therefore conclude that, *if* $X(HCN)$ *remains fixed*, $X(HCO^+)$ must be enhanced by at least a factor of 3 in the outflow lobe, compared to the quiescent cloud. This enhancement estimate is a lower limit as, by calculating a velocity-averaged abundance ratio, we have effectively diluted any enhancement in the high-velocity wing component by adding in emission from the line-core component which, as shown in Figure 6*b*, is relatively insensitive to the presence of the outflow lobe.

Together, the above analyses suggest that the fractional abundance of HCO^+ is enhanced in the DR 21 outflow lobes, relative to that in the quiescent cloud, by a factor of between 3 and 10.

3.6. *Column Density of* H_2

Knowledge of the fractional abundance of HCO^+, together with the expression for the total beam-averaged column density of HCO^+ (eq. [6]), leads to an estimate of the column density of molecular gas:

$$\bar{N}(H_2) = \frac{1}{X(HCO^+)} \bar{N}_{tot}(HCO^+) . \quad (9)$$

To calculate the peak column density of molecular gas in the DR 21 outflow lobes from the HCO^+ observations presented here, we treat the low- and high-velocity components of the HCO^+ profile separately using $X(HCO^+) \approx 6 \times 10^{-9}$ and 4×10^{-10} for the high- and low-velocity components, respectively, as determined in the previous section. Summing the column densities of both velocity components results in peak column densities of $5 \times 10^{22} \leq \bar{N}(H_2) \leq 10^{23}$ cm^{-2} toward the brightest clumps of HCO^+ emission in both outflow lobes. This result shows reasonable agreement with the column density calculated by Garden et al. (1986) and Nadeau et al. (1991) from estimates of the near-infrared extinction to the H_2 outflow lobes: i.e., $\bar{N}(H_2) \approx 3 \times 10^{22}$ cm^{-2}.

3.7. *Mass of Molecular Gas*

Although the mass of gas can be calculated from the beam-averaged column density (eq. [9]), we prefer to use a more direct method which does not require the use of a beam-filling factor. For optically thin emission (see § 3.3), the flux received from an isotropically emitting source at distance D from Earth is

$$\int S_\nu \, dv = \frac{N_u A_{10} h\nu}{4\pi D^2} \text{ ergs s}^{-1} \text{ cm}^{-2} , \quad (10)$$

where S_ν is the flux received per unit frequency and N_u is the number of molecules in the upper state. Changing from fre-

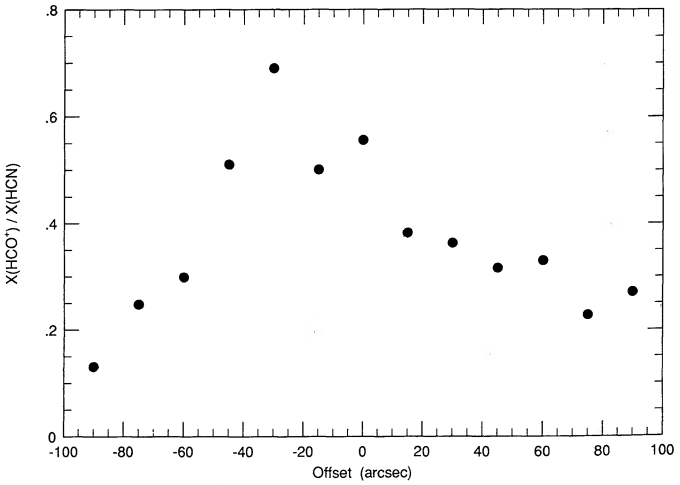

FIG. 7.—Values of $X(HCO^+)/X(HCN)$, averaged over the entire line profile, along a N-S cut centered on the peak of high-velocity HCO^+ emission from the western outflow lobe.

quency to velocity units and substituting $A_{10} = 5.5 \times 10^{-5}$ s^{-1} for the HCO^+ $J = 1$–0 line (Blake et al. 1987) then gives

$$N_u = 9.87 \times 10^{46} \left(\frac{S_\nu}{Jy}\right)\left(\frac{\Delta v}{\text{km s}^{-1}}\right), \quad (11)$$

where S_ν is the average flux within the velocity interval Δv, and we have assumed $D = 3$ kpc for the distance to the DR 21 outflow. To calculate the total number of HCO^+ molecules, $N_{\rm tot}$, we need to divide N_u by the fraction of molecules that are in the upper state, f_u. If we assume that the gas is in local thermodynamic equilibrium (LTE), the value of f_u can be estimated from the Boltzmann distribution:

$$f_u = \frac{g_u}{U} \exp\left[-\frac{hBJ_u(J_u+1)}{kT_{\rm ex}}\right], \quad (12)$$

where $J_u = J + 1$, B is the rotational constant [$= \nu/2J_u$], g_u is the degeneracy of the upper level ($= 2J_u + 1$), and U is the partition function, which for a linear molecule can be approximated by $U = kT_{\rm ex}/hB$ (see appendix of Garden et al. 1991b). For an excitation temperature of $T_{\rm ex} = 30$ K, we obtain $f_u = 0.185$, and

$$N_{\rm tot} = \frac{N_u}{f_u} = 5.32 \times 10^{47} \left(\frac{S_\nu}{Jy}\right)\left(\frac{\Delta v}{\text{km s}^{-1}}\right). \quad (13)$$

The total mass of molecular gas is then calculated as follows:

$$M(\text{mol. gas}) = \frac{N_{\rm tot}}{X(HCO^+)}\, \mu_g\, m(H_2)\,. \quad (14)$$

Substituting $\mu_g = 1.36$ for the mean atomic weight, we arrive at the desired result:

$$M(\text{mol. gas}) = \frac{1.21 \times 10^{-9}}{X(HCO^+)} \left(\frac{S_\nu}{Jy}\right)\left(\frac{\Delta v}{\text{km s}^{-1}}\right) M_\odot\,. \quad (15)$$

Using the above equation, we have calculated the total mass of gas associated with the low- and high-velocity components of the HCO^+ emission in the eastern and western outflow lobes. The results of these calculations are shown in Table 1. In summary, we find that the total mass of gas in both outflow lobes is of order $1000 \rightarrow 2700$ $M_\odot$, with $\sim$90% of the total mass residing in the low-velocity component.

The major source of uncertainty in our calculation of the masses given in Table 1 is the error associated with our estimate of $X(HCO^+)$, which could be as much as an order of magnitude depending on the validity of the basic assumptions employed in deriving this important quantity. However, the close agreement between our estimate of the outflow mass and the independent estimate of Garden et al. (1991b), from single-dish observations of the CO $J = 1$–0 line, suggests that our estimate of a few thousand $M_\odot$ is probably close to the real value.

To calculate the kinetic energy (E_k) associated with each velocity component, we assume that the outflow mass is evenly distributed in velocity within each component, in which case

$$E_k = \int_{v_1}^{v_2} \frac{1}{2} \frac{M_{v_1,v_2}}{(v_2 - v_1)}\, v^2\, dv\,. \quad (16)$$

In the above equation v_1 and v_2 are the lower and upper velocity limits, measured with respect to the cloud rest velocity, of a particular velocity component and M_{v_1,v_2} is the total mass associated with that component. After integrating, we obtain

$$E_k = \frac{1}{6} M_{v_1,v_2} \frac{(v_2^3 - v_1^3)}{(v_2 - v_1)}\,. \quad (17)$$

Our best estimate of the total outflow kinetic energy, as shown in Table 1, lies between 1×10^{48} and 2×10^{48} ergs. Once again, this result shows good agreement with the independent estimate of Garden et al. (1991b).

3.8. *Preliminary* HCO^+ $J = 4$–3 *Observations*

To test the feasibility of mapping the dense gas in the DR 21 outflow in the $J = 4$–3 transition of HCO^+, we used the Caltech Submillimeter Observatory[4] (CSO) in 1991 July to obtain spectra toward three positions coincident with the peaks of HCO^+ $J = 1$–0 line emission in the east and west high-velocity outflow lobes, and the central low-velocity source. These preliminary $J = 4$–3 spectra are shown in Figure 8, along with corresponding $J = 1$–0 spectra made from the Hat Creek interferometer data with a synthesized 20″ beam to match the CSO observations. The brightness of the $J = 4$–3 spectra have been corrected for the 60% main beam efficiency, but the absolute uncertainly is of order 50%, mainly due to the unknown sideband ratio.

In a similar manner to the $J = 1$–0 emission, the $J = 4$–3 profiles toward the east and west outflow lobes are broad with

[4] The CSO is operated by the California Institute of Technology under funding from the NSF, contract AST 83-11849.

TABLE 1

OUTFLOW MASS AND KINETIC ENERGY

LOBE(S)	COMPONENT: High-Velocity Blue $v_{\rm lsr} = -27.5$, $\Delta v = 30$	Low-Velocity $v_{\rm lsr} = -5$, $\Delta v = 15$	High-Velocity Red $v_{\rm lsr} = 17.5$, $\Delta v = 30$	TOTAL
		Mass ($M_\odot$)		
West lobe	$50 \rightarrow 95$	$540 \rightarrow 1350$	$30 \rightarrow 60$	$620 \rightarrow 1505$
East lobe	$35 \rightarrow 70$	$420 \rightarrow 1045$	$25 \rightarrow 50$	$480 \rightarrow 1165$
Both lobes	$85 \rightarrow 165$	$960 \rightarrow 2395$	$55 \rightarrow 110$	$1100 \rightarrow 2670$
		Kinetic Energy (ergs)		
Both lobes	$5.0 \rightarrow 9.5 \times 10^{47}$	$1.8 \rightarrow 4.5 \times 10^{47}$	$3.2 \rightarrow 6.4 \times 10^{47}$	$1.0 \rightarrow 2.0 \times 10^{48}$

NOTE.—For calculating the above masses we have assumed $4 \times 10^{-9} \leq X(HCO^+) \leq 8 \times 10^{-9}$ for the high-velocity components and $2 \times 10^{-10} \leq X(HCO^+) \leq 5 \times 10^{-10}$, for the low-velocity component, as estimated in § 3.4.

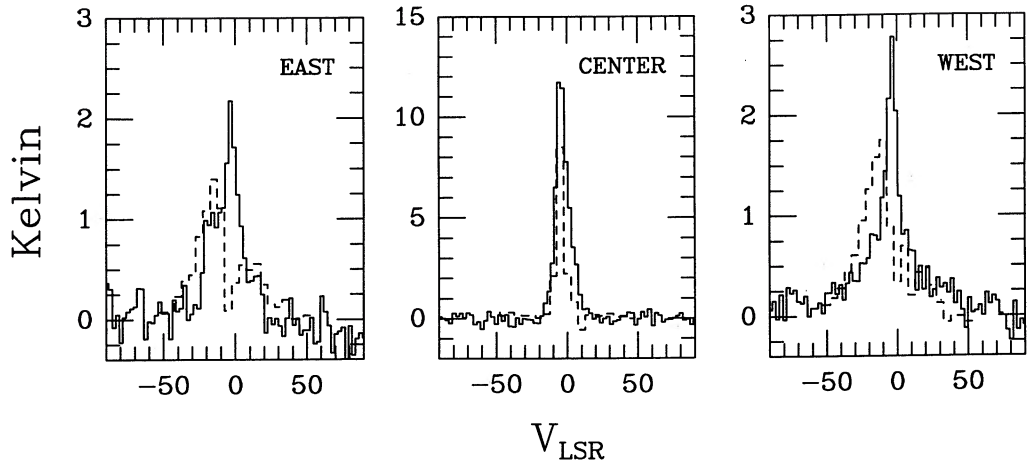

FIG. 8.—Profiles of HCO^+ $J = 4$–3 (*solid lines*) and $J = 1$–0 (*dashed lines*) emission toward the peaks of HCO^+ $J = 1$–0 line emission in the east and west outflow lobes, and the central source. The HCO^+ $J = 4$–3 spectra were obtained using the Caltech Submillimeter Observatory with a beam size of 20″. The $J = 1$–0 spectra were synthesized for a 20″ beam from the Hat Creek interferometer data.

distinct high-velocity wings which extend out to ± 50 km s^{-1} from the line core, while the profile of the central source is relatively narrow with no detectable wing component. However, in contrast to the $J = 1$–0 emission, the $J = 4$–3 profiles are characterized by a bright, low-velocity spike component. The apparent absence of a similar component in the $J = 1$–0 profiles most likely results from the fact that the low-velocity component is probably extended on scales significantly larger than sampled by the *u-v* coverage, causing the interferometer to reslove out the low-velocity emission. Indeed, the $J = 1$–0 emission almost drops to zero at the same velocity corresponding to the spike component of the $J = 4$–3 profiles, as would be expected if the $J = 1$–0 interferometer data were plagued by missing flux close to the rest velocity of the DR 21 molecular cloud (~ -2.5 km s^{-1}).

We only wish to point out here that the detection of broad wings in the $J = 4$–3 profiles suggests the presence of extremely dense ($n \geq 10^7$ cm^{-3}) gas within the DR 21 outflow. Presumably this dense gas is in the form of many small clumps which have been compressed and ram-pressure accelerated on interaction with a powerful stellar wind (Garden et al. 1991b).

4. DISCUSSION

4.1. *The Central Source*

To obtain a clearer picture of the spatial relationship between the central HCO^+ source and the DR 21 compact H II region, we show in Figure 9 a superposition of the 89 GHz continuum (Fig. 1) on the contours of integrated HCO^+ emission from the central field (Fig. 3). The most striking feature seen in this comparison is the distinct anticorrelation in the spatial distribution of the continuum emission (which traces the ionized gas) and the HCO^+ emission. Although the subtraction of the continuum emission from the line maps may be partially responsible for the anticorrelation and observed ring like morphology, we are convinced that the several distinct clumps that border the H II region are real, as is the break in the molecular ring to the north, where the northern H II component (D) connects with the southern H II components (A, B and C). The close connection between the ionized and dense molecular gas components suggests that the molecular ring traces ambient gas that has been swept up by a slow shock preceding the expanding H II region. The narrow line widths observed toward the central HCO^+ source (see spectrum 3 of Fig. 4) lend further evidence in favor of the expanding H II region scenario. Our results agree well with those of Dickel et al. (1985) who also find in HCN $J = 1$–0 emission a bright clump southwest of the H II region, at the same position as the brightest clump seen here in HCO^+. The low sensitivity of their observations, however, precluded the detection of the fainter clumps that comprise the molecular ring. Assuming optically thin emission, we calculate a mass for the bright southwestern clump of between 100 and 800 $M_\odot$, depending on the value chosen for the HCO^+ abundance.

High angular resolution NH_3 spectral line observations of the southwestern clump show Doppler shifts consistent with gravitational collapse onto a core of mass ~ 300 $M_\odot$ (Keto 1990), in good agreement with our mass estimate. It is therefore conceivable that this massive clump may be a prime example of a young protostellar condensation in its earliest stages of for-

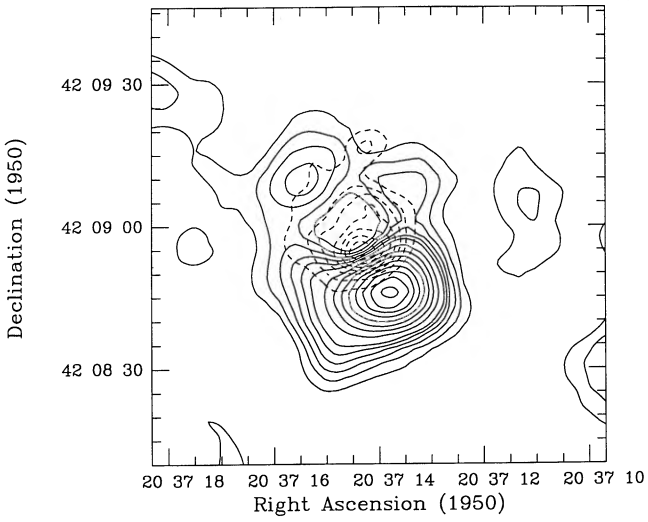

FIG. 9.—Superposition of contours of 89 GHz continuum emission (*dashed lines*), as shown in Fig. 1, on contours of integrated HCO^+ $J = 1$–0 emission (*solid lines*) toward the DR 21 cloud core. The contour interval is 0.25 Jy beam^{-1} for the continuum and 4.5 Jy km s^{-1} beam^{-1} × 1, 2, 3, 4, 5, 6, 8, 10, 12, 14, 16, 18, 20, 22 for the HCO^+ emission. The beam sizes are 5.″6 × 5.″3 and 10.″3 × 9.″4 for the continuum and line emission, respectively.

mation. However, recent observations (J. E. Carlstrom, private communication) obtained using the Caltech Submillimeter Observatory show the presence of a compact region of broad SiO $J = 5$–4 emission coincident with the southwestern clump. The presence of the high-velocity SiO emission, which is known to be a reliable signature of molecular outflows, suggests that a young star may have already formed in the southwestern clump. It is therefore possible that this clump may contain the driving source of the energetic DR 21 outflow. Clearly, a more detailed kinematic study, at higher angular resolution than afforded by the current observations, is required to investigate whether the outflow, as traced by the SiO emission is directly associated with the massive DR 21 outflow, and whether the compression of the ambient cloud medium by the expanding H II region plays an important role in stimulating secondary star formation.

4.1. *The Central Gap*

It is puzzling that there is no indication of high-velocity HCO^+ emission associated with the central source which might have been expected if the source of the observed high-velocity outflow were to reside within the DR 21 cloud core. As remarked upon in § 3.2, the absence of high-velocity HCO^+ emission from the central field creates a gap in the HCO^+ emission between the central source and the outflow lobes (see Fig. 3). A similar gap is also seen in shock-excited H_2 line emission (Garden et al. 1991a). A simple solution to this puzzle may be devised in which the stellar wind, which drives the high-velocity outflows, is permitted to vary with time. For example, if the stellar wind were to have switched off a few thousand years ago, the period of inactivity from then to the present time would produce a central gap in the outflow of sufficient size to explain the central hole seen in the high-velocity HCO^+ line emission. In effect, the extended outflow lobes would then represent the fossil remnants of an earlier phase of energetic mass loss. However, recent observations of neutral hydrogen (Russell 1989) and CO line emission (Garden et al. 1991b) reveal high-velocity emission indicative of mass outflow within the central gap. These results thus prove that the DR 21 outflow source is still currently active and that the central gap observed in high-velocity HCO^+ emission probably does not reflect a recent turn off of the driving mechanism.

In view of the noted sensitivity of HCO^+ emission to shocks (see § 3.4), we suggest an alternative scenario in which the observed absence of high-velocity HCO^+ and H_2 line emission toward the core of the DR 21 cloud results from a *lack of strong shocks* in that region. Such a situation may arise if the outflow, close to the driving source, is sufficiently well collimated (i.e., a jet) and the core medium is sufficiently homogeneous that the high-velocity gas is propelled outward along a preexisting channel, or cavity, with minimal interaction. The high-velocity HCO^+ line emission from the outflow thus remains weak and difficult to detect until, at some point farther out in the cloud, the outflow collides with dense clumps in the ambient cloud medium, giving rise to luminous shocks. It is these outflow/ambient clump shocks that are highlighted in H_2 and HCO^+ line emission. Direct evidence for the interaction of the high-velocity outflow with dense clumps in the ambient cloud medium will be presented and discussed further in § 4.4.

A major problem with the above scenario, however, is that, if the central driving mechanism is currently active, it is impossible for the DR 21 compact H II region to be related to the outflow since the large mass-loss rates ($\dot{M} \approx 10^{-3}\ M_\odot\ \mathrm{yr}^{-1}$; Garden et al. 1991b) would quench the ionizing photons and thus prevent the formation of an H II region. The only way out of this predicament is to propose that the DR 21 H II region is not directly involved with the outflow phenomenon but is, instead, a chance projection along the line of sight. For example, we can envisage a situation where the extended outflow source is located close to the center of the DR 21 cloud core while the H II region is located on the back surface of the cloud. Although it is tempting to solve the problem by dispensing with the H II region, the solution is probably not this simple as the central location of the H II region with respect to the extended outflow lobes suggests a causal connection between the two. Unfortunately, a solution to this vexing problem must await future high-resolution spectral line observations of the ionized gas within the DR 21 H II region which may help determine the relative location of the H II region with respect to the DR 21 outflow.

4.3. *Comparison with Shock-excited* H_2 *Line Emission*

One of the main goals of this observing project is to compare the distribution of the dense ambient cloud gas in the DR 21 outflow lobes with the distribution of the hot, shocked gas as probed by vibrationally excited H_2 line emission (Garden et al. 1986, 1990, 1991a). In order to conduct such a comparison, we show in Figure 10 a 1″ resolution image of H_2 $v = 1$–0 $S(1)$ line emission (Garden et al. 1990) superposed on the contours of integrated HCO^+ emission, as presented previously in Figure 3. The outcome of this comparison is striking; the shock-excited H_2 and the HCO^+ line emission exhibit an almost identical spatial distribution. The peaks of emission are slightly displaced, but the more diffuse emission appears to be spatially correlated over both outflow lobes. The displacement of the peaks of line emission presumably arises from the fact that the H_2 and HCO^+ lines probe gas of dramatically different temperatures. The H_2 emission comes from the immediate shock front while the HCO^+ emission originates from either the preshock ambient medium or from postshock gas that lies sufficiently far downstream to have had time to cool to temperatures < 100 K. Nonetheless, the remarkable similarity in the global appearance of both emission lines suggests that the HCO^+ emission associated with the DR 21 outflow lobes is strongly influenced by the same shocks that give rise to the bright H_2 line emission. In conjunction with the observed enhancement in the HCO^+ fractional abundance (see § 3.4), the above spatial correlation strongly suggests that high-velocity HCO^+ emission is a sensitive tracer of the morphology and dynamics of shocks in the densest regions of the interstellar medium. Similar spatial correlations between HCO^+ $J = 1$–0 and H_2 $v = 1$–0 $S(1)$ line emission have been reported previously for the Orion (Vogel et al. 1984) and NGC 2071 (Kitamura et al. 1990) molecular outflows. These authors similarly speculate that the observed correlation may originate from an enhancement in the excitation and/or fractional abundance of the HCO^+ ion within the warm gas comprising the shock-heated outflow lobes.

In closing this section, we note that a direct spatial correlation between the infrared H_2 and millimeter HCO^+ line emission is predicted by the time-dependent shock model of Wolfire & Königl (1992). As was discussed in § 3.4, the Wolfire & Königl model, which is specific to the conditions inherent to Herbig-Haro objects, can also explain the observed enhancement in HCO^+ abundance. Considering the high velocities

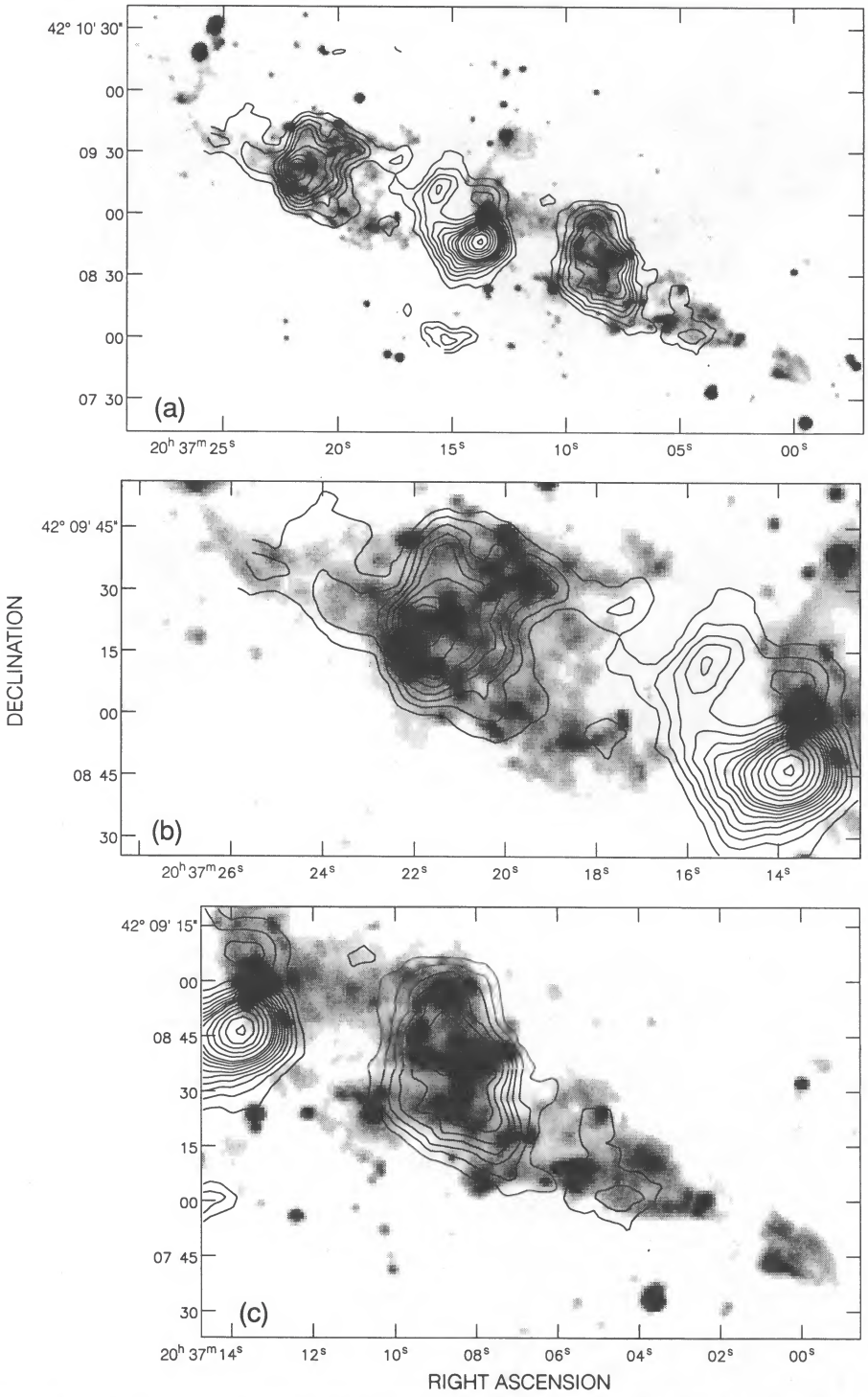

FIG. 10.—Superposition of the contours of HCO^+ $J = 1$–0 integrated intensity (see Fig. 3) on a gray-scale map of shock-excited H_2 $v = 1$–0 line emission as observed by Garden et al. (1990): (*a*) entire outflow region; (*b*) detail of east lobe; (*c*) detail of west lobe. The contours are 4.5 Jy km s^{-1} $beam^{-1}$ × 1, 2, 3, 4, 5, 6, 7, 8, 9, 10, 12, 14, 16, 18, 20.

associated with, and clumpy structure of, the DR 21 outflow lobes (Garden et al. 1990, 1991a), it is tempting to speculate that the outflow lobes may be composed of many super-luminous Herbig-Haro type objects that possess most of the expected infrared and millimeter signatures but lack the telltale optical line emission due to heavy foreground extinction.

4.4. *The Dynamics of the Outflow Lobes*

In order to study in more detail the motions of the gas within the DR 21 outflow lobes, we have constructed velocity-channel plots of the low- and high-velocity emission (see Table 1) from the east and west outflow lobes, as shown in Figure 11.

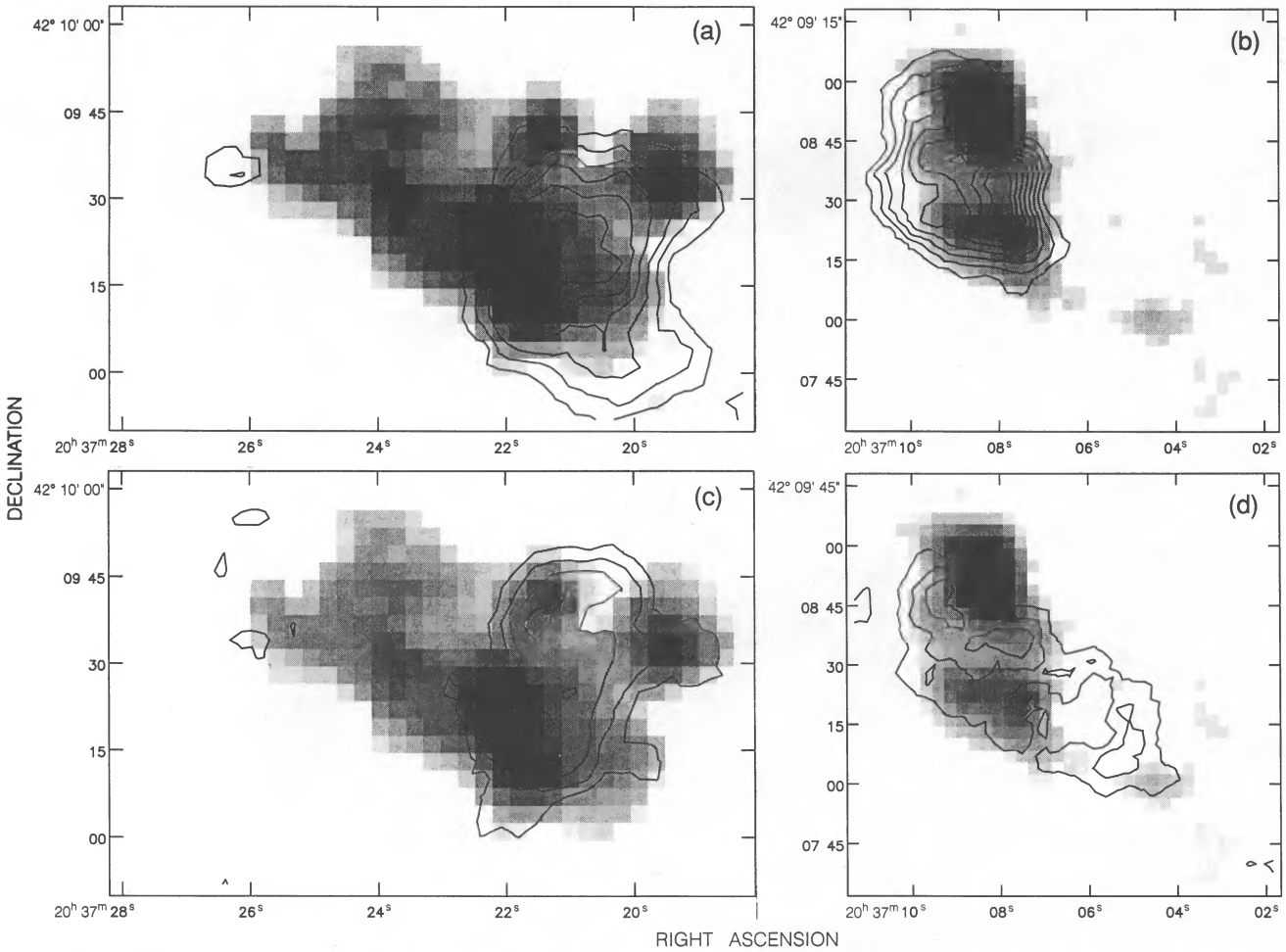

FIG. 11.—Superposition of contours of high-velocity blueshifted (-42.5 to -12.5 km s^{-1}) HCO^+ $J = 1$–0 emission on a gray-scale map of low-velocity (-12.5 to 2.5 km s^{-1}) HCO^+ emission from (*a*) the eastern outflow lobe and (*b*) the western outflow lobe. Contours of high-velocity redshifted (2.5 to 32.5 km s^{-1}) HCO^+ emission on the same gray-scale maps of the low-velocity emission from (*c*) the eastern outflow lobe and (*d*) the western outflow lobe. The contours are 3.0 Jy km s^{-1} beam^{-1} × 1, 2, 3, 4, 5, 6, 7, 8, 9. The triangle denotes the DR 21-W methanol maser recently discovered by Plambeck & Menten (1990).

With the exception of the high-velocity redshifted emission from the eastern outflow lobe (Fig. 11*c*), these figures clearly show that the high-velocity gas in both outflow lobes tends to be more streamlined than the low-velocity gas with the peaks of high-velocity emission lying between the peaks of low-velocity emission. Such a morphology is expected if the low-velocity emission arises from a shell of swept-up ambient gas that surrounds a high-velocity wind. The high-velocity emission may then originate from dense clumps of gas that have been entrained into the high-velocity wind from the outflow walls. The interaction between the high-velocity wind and the ambient cloud is especially prominent in Figures 11*b* and 11*d* which show a superposition of the high- and low-velocity components in the western outflow lobe. Here we see that a bright clump of dense, low-velocity gas has formed at the edge of the outflow lobe. The high-velocity wind apparently impacts, and is deflected by, this massive clump; a sharp bend at this position is also seen in H_2 maps of the western outflow lobe (Garden et al. 1990, 1991a). Furthermore, we propose that on impacting the massive clump, the direction of propagation of the wind is suddenly changed, giving rise to the anomalous shift in the radial velocity of the HCO^+ line previously noted in § 3.2. Further evidence in support of the wind/clump collision scenario derives from the recent detection of a bright 95 GHz methanol maser in the western lobe of the DR 21 outflow (Plambeck & Menten 1990), which, as shown in Figure 11, lies directly between the low-velocity HCO^+ clump and the high-velocity HCO^+ emission. As originally proposed by Plambeck & Menten, this exciting result suggests that the DR 21 methanol maser is formed where the high-velocity wind shocks a preexisting dense clump in the surrounding ambient cloud medium. This discovery is important because it shows that the density structure of the ambient cloud medium can play a major role in shaping both the morphology and velocity structure of young stellar outflows.

5. SUMMARY

We have used the Hat Creek millimeter array to study the spatial and velocity distribution of HCO^+ $J = 1$–0 line emission from the ultraluminous DR 21 outflow source. The main results of these observations are as follows:

1. The brightest and narrowest lines arise from a dense clump of emission located at the southwestern edge of the central DR 21 H II region. Several fainter clumps are detected at other positions around the H II region. We propose that

these low-velocity clumps are formed by the expanding H II region as it sweeps up and compresses the surrounding ambient cloud medium.

2. Extended, high-velocity HCO^+ emission is detected from both outflow lobes. There is a strong correlation between the spatial distribution of high-velocity HCO^+ and shock-excited H_2 line emission.

3. The detection of bright, high-velocity HCO^+ $J = 4$–3 emission suggests the presence of extremely dense gas ($n \geq 10^7$ cm^{-3}) within the outflow lobes. This dense gas may assume the form of many small clumps which have been ram pressure–accelerated on interaction with a powerful stellar wind.

4. From a detailed study of the ratio of HCO^+ to ^{13}CO and HCN line brightness across the western outflow lobe, we find that the fractional abundance of high-velocity HCO^+ may be enhanced by a factor of between 3 and 10 compared to the quiescent cloud. Together with the striking spatial correlation between high-velocity HCO^+ and shock-excited H_2 line emission, this result suggests that the enhanced fractional abundance of high-velocity HCO^+ may result from increased ionization following the passage of a strong shock.

5. Both the appearance and dynamical structure of the western outflow lobe indicate that collisions between the outflow and clumps within the ambient cloud medium play an active role in controlling the dynamical evolution of the outflow.

6. We suggest that the central gap in the distribution of high-velocity HCO^+ and H_2 line emission results from the absence of strong shocks in that region. Such a situation could arise if the stellar wind close to the central driving engine is sufficiently well collimated, and the surrounding cloud medium is sufficiently homogeneous, that the wind propagates outward along a preexisting channel, or cavity, without shocking the surrounding cloud medium.

7. These observations confirm our earlier claim that the DR 21 star-forming complex harbors one of the most energetic young stellar outflows yet discovered in the Galaxy.

We would like to thank Alex Rudolph for helpful discussions and the referee for helpful comments.

R. P. G. acknowledges support from the Alfred P. Sloan Foundation and the California Space Institute. Research at the University of California, Berkeley, Radio Astronomy Laboratory is supported in part by NSF grant AST 87-14721.

REFERENCES

Blake, G. A., Sutton, E. C., Masson, C. R., & Phillips, T. G. 1987, ApJ, 315, 621
Campbell, M. F., Hoffmann, W. F., Thronson, H. A., Jr., Niles, D., Nawfel, R., & Hawrylycz, M. 1982, ApJ, 261, 550
Dickel, H. R., Goss, W. M., Rots, A. H., & Blount, H. M. 1986, A&A, 162, 221
Dickel, H. R., Ho, P. T. P., & Wright, M. C. H. 1985, ApJ, 290, 256
Dickel, H. R., Lubenow, A. F., Goss, W. M., Forster, J. R., & Rots, A. H. 1983, A&A, 120, 74
Dickel, J. R., Dickel, H. R., & Wilson, W. J. 1978, ApJ, 223, 840
Dickinson, D. F., Rodriguez-Kuiper, E. N., Dinger, A. S., & Kuiper, T. B. H. 1980, ApJ, 237, L43
Elitzur, M. 1983, ApJ, 267, 174
Fischer, J., Sanders, D. B., Simon, M., & Solomon, P. M. 1985, ApJ, 293, 508
Garden, R. P. 1987, Ph.D. thesis, Univ. of Edinburgh
Garden, R. P., Geballe, T. R., Gatley, I., & Nadeau, D. 1986, MNRAS, 220, 203
———. 1991a, ApJ, 366, 474
Garden, R. P., Russell, A. P. G., & Hayashi, T. 1992, in preparation
Garden, R. P., Hayashi, M., Gatley, I., Hasegawa, T., & Kaifu, N. 1991b, ApJ, 374, 540
Garden, R. P., Russell, A. P. G., & Burton, M. G. 1990, ApJ, 354, 232
Haese, N. N., & Woods, R. C. 1979, Chem. Phys. Lett., 61, 396
Harris, S. 1973, MNRAS, 162, 5P
Harvey, P. M., Joy, M., Lester, D. F., & Wilking, B. A. 1986, ApJ, 300, 737
Harvey, P. M., Campbell, M. F., & Hoffmann, W. F. 1977, ApJ, 211, 786
Iglesias, E., & Silk, J. 1978, ApJ, 226, 851
Keto, E. R. 1990, ApJ, 350, 722
Kitamura, Y., Kawabe, R., Yamashita, T., & Hayashi, M. 1990, ApJ, 363, 180
Kuiper, T. B. H., Zuckerman, B., & Rodriguez-Kuiper, E. N. 1981, ApJ, 251, 88
Lang, K. R. 1980, Astrophysical Formulae (Berlin: Springer)
Lizano, S., Heiles, C., Rodriguez, L. F., Koo, B. C., Shu, F. H., Hasegawa, T., Hayashi, S., & Mirabel, I. F. 1988, ApJ, 328, 763
Loren, R. B., Wootten, A., Sandquist, A., Friberg, P., & Hjalmarson, A. 1984, ApJ, 287, 707
Mitchell, G. F. 1984, ApJ, 287, 665
Nadeau, D., Riopel, M., & Geballe, T. R. G. 1991, ApJ, 372, L103
Phillips, T. G., Knapp, G. G., Huggins, P. J., Werner, M. W., Wannier, P. G., Neugebauer, G., & Ennis, D. 1981, ApJ, 245, 512
Plambeck, R. L., & Menten, K. M. 1990, ApJ, 364, 555
Pratap, P., Batrla, W., & Snyder, L. E. 1990, ApJ, 351, 530
Richardson, K., Sandell, G., & Krisciunas, K. 1989, A&A, 244, 199
Richardson, K. J., White, G. J., Avery, L. W., Lesurf, J. C. G., & Harten, R. H. 1985, ApJ, 290, 637
Righini-Cohen, G., Simon, M., & Young, E. T. 1979, ApJ, 232, 782
Roelfsema, P. R., Goss, W. M., & Geballe, T. R. 1989, A&A, 222, 247
Russell, A. P. G. 1990, in Submillimeter Astronomy, ed. G. D. Watt & A. S. Webster (Dordrecht: Kluwer), 281
Vogel, S. N., Wright, M. C. H., Plambeck, R. L., & Welch, W. J. 1984, ApJ, 238, 655
White, G. J., Rainey, R., Hayashi, S. S., & Kaifu, N. 1987, A&A, 173, 337
Wolfire, M. G., & Königl, A. 1992, in preparation
Wootten, A., Loren, R. B., Sandquist, A., Friberg, P., & Hjalmarson, A. 1984, ApJ, 279, 633
Ziurys, L. M., Snell, R. L., & Dickman, R. L. 1989, ApJ, 341, 857